IEEE Access
Multidisciplinary ⋮ Rapid Review ⋮ Open Access Journal

Received 10 April 2026, accepted 28 April 2026, date of publication 4 May 2026, date of current version 8 May 2026.

Digital Object Identifier 10.1109/ACCESS.2026.3690197

RESEARCH ARTICLE

On the Improvement of Gate Fidelity in Spin Qubits With Two-Level Fluctuators at Higher Temperatures

YUDAI SATO[1,2], HIDEHIRO ASAI[2], (Member, IEEE), TAKAHIRO MORI[2], (Member, IEEE), AND TAKAYUKI KAWAHARA[1], (Life Fellow, IEEE)

[1]Tokyo University of Science, Tokyo 125-8585, Japan
[2]National Institute of Advanced Industrial Science and Technology (AIST), Tsukuba 305-8568, Japan

Corresponding authors: Yudai Sato (4324529@ed.tus.ac.jp) and Takahiro Mori (mori-takahiro@aist.go.jp)

This work was supported in part by the Ministry of Education, Culture, Sports, Science and Technology (MEXT) Quantum Leap Flagship Program (Q-LEAP), Japan, under Grant JPMXS0118069228.

ABSTRACT The importance of the role of two-level fluctuators (TLFs) in causing qubit frequency (f_q) shifts has been highlighted in previous studies to improve the gate fidelity in silicon spin qubits at higher temperatures. In this study, we employed a simulation technique to investigate the origin of the temperature dependence of f_q shifts in silicon spin qubits. Among the various possible microscopic origins, we focused on the charge noise, which is attributed to the TLFs at the semiconductor/oxide interface, for which the experimental features of the f_q shift have been theoretically reproduced in previous studies. We analyze the TLF characteristics required to improve the gate fidelity by simulating the effect of charge noise, considering the spatial and energetic distributions, as well as characteristic parameters. We observed that the exponential distribution of the activation energies was preferable for reproducing the f_q shift and fidelity improvement. Moreover, in terms of parameter selection, a short transition time and a steep temperature transition can improve fidelity during higher-temperature operations. Based on these findings, we discussed the origin of TLFs and observed that electronic transitions are more likely to produce TLFs than transitions involving atomic displacement.

INDEX TERMS Quantum computer, Si spin qubit, charge noise.

I. INTRODUCTION

Electrons confined within quantum dots exhibit a spin-1/2 degree of freedom that can be utilized as qubits [1]. These spin qubits, particularly those based on semiconductor silicon, represent a promising quantum computing platform owing to their long coherence times and compatibility with advanced semiconductor manufacturing technologies [2]. Advances in isotopic purification and control techniques have enabled high-fidelity operations for both single-qubit gates [3], [4], [5], [6], [7], [8] and two-qubit gates [5], [6], [7], achieving gate fidelities that surpass the threshold required for surface code quantum error correction [9], [10]. As the next step, the variation issues in gate fidelity must be considered for each integrated qubit device for the large-scale integration of such spin qubits required to achieve practical fault-tolerant quantum computers.

One of the key challenges arises from the temperature dependence of the Larmor frequency (f_q), also referred to as the qubit frequency. The f_q value corresponds to the energy difference between the up and down spin states, which are determined by Zeeman splitting due to an external magnetic field required for spin qubit operation. Ideally, for microwave-driven qubit operation, the f_q value must remain constant to maintain the resonance condition between the f_q value and microwave frequency. However, some experiments demonstrated that the f_q value can shift during operation by approximately 1 MHz, either positively or negatively, depending on the devices [3], [11], [12], [13]. Recent studies reported that the f_q shift arises from the microwaves

The associate editor coordinating the review of this manuscript and approving it for publication was Siddhartha Bhattacharyya.

used to operate the device, which emits heat [14]. Additionally, this shift exhibited non-monotonic behavior, featuring a sharp increase at low temperatures, followed by a gradual decrease at higher temperatures. Consequently, the temperature dependence of f_q disrupts the resonance condition, thereby deteriorating the gate fidelity during operation.

Undseth et al. reported that operating the qubits at a higher temperature of 200 mK rather than the standard temperature of approximately 20 mK can mitigate the effect of the f_q shift on the gate fidelity [14]. Consequently, they achieved better gate fidelity at 200 mK than at 20 mK in the Si/SiGe spin qubit devices.

These studies demonstrated key features of the f_q shift that deteriorate the gate fidelity, which are as follows:

1. The f_q value can shift both positively and negatively,
2. The f_q shift exhibits non-monotonic temperature dependence,
3. The microwave produces heat, in which causes the f_q shift,
4. Higher-temperature operations can mitigate the f_q shift.

However, the microscopic origin of the f_q shift remains unclear. Several candidates have been proposed to this end. The first candidate is the strain caused by the temperature change, which can, in turn, vary the confinement potential and shift the center position of the electron [3]. Such a shift can lead to changes in the f_q value in the presence of magnetic field gradients. The second candidate is the temperature-dependent variation in the electron g-factor, which directly determines the qubit frequency via $f_q = g\mu_B B/\hbar$, where g is the electron g-factor, μ_B is the Bohr magneton, B is the external magnetic field, and $\hbar$ is the reduced Plank constant [14]. The effective g-factor depends on various factors including spin-orbit coupling, the shape of the confinement potential, valley state, crystal composition and strain, each of which can exhibit temperature dependence and therefore contribute to changes in f_q. The third candidate is charge noise arising from the thermally fluctuating two-level fluctuators (TLFs) at the semiconductor/oxide interface, which can influence the electron position via Coulomb interaction and then cause the f_q shift based on the analogy of the first case [14], [15], [16]. Subsequently, Choi and Joynt reported that the theoretical charge-noise model could reproduce the other key features of the f_q shift, i.e., the sign-indefinite and non-monotonic temperature dependence, by considering the uniform distribution of TLFs around a qubit [16]. Finally, although the temperature dependence of nuclear spins or unpaired electron spins could induce f_q shifts, their contributions are expected to be too small to account for the experimentally observed behavior. Thus, they are unlikely to represent the microscopic origin of the measured f_q shifts [14].

In this study, we focused on the charge noise model and analyzed the origin of TLFs to provide feedback on the qubit fabrication. We analyzed the origins of the TLFs from several perspectives regarding the spin qubit operation. One example corresponds to the defects in the gate oxide, for which several atomistic mechanisms have been proposed as potential

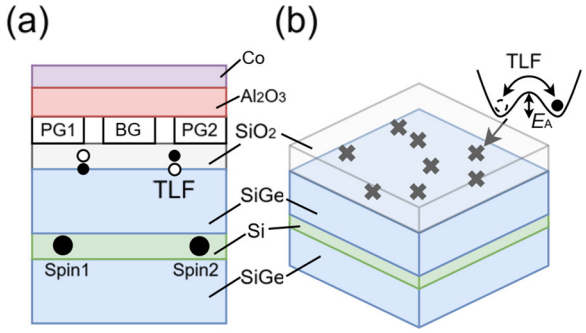

FIGURE 1. Schematic diagrams of the Si/SiGe gate-defined quantum dot device structure assumed in this work. (a) Cross-sectional view showing the typical layer structure of the assumed Si/SiGe device. (b) Bird's-eye view illustrating the TLFs distributed at the interface between the semiconductor and insulator.

sources of TLFs. These include tunneling atoms, hydrogen rotations, and collective atomic motion [17]. In theoretical studies that focused on the semiconductor/oxide interface, various types of trap centers associated with oxide and hydrogen atoms have been considered as the possible sources of TLFs. These hypotheses were supported by a comparison between the energy levels predicted via DFT calculations and those obtained from experimental measurements [18], [19], [20]. Furthermore, noise measurements conducted at cryogenic temperatures indicate that the band-edge states induced by random potentials can cause $1/f$ noise produced by random telegraph noise, which is considered a type of TLFs [21], [22], [23].

To this end, we considered them in our theoretical calculations as the actual TLFs are randomly distributed in space around a qubit and in energy. The study was conducted in three steps. First, we established a charge noise model originating from the TLFs, considering their spatial and energetic distributions. This step is similar to the previous study conducted by Choi and Joynt [16], except that we additionally considered some types of distribution. Second, we narrowed down the TLF characteristics as the key features of the f_q shift mentioned above were reproduced. This step helped obtain the most plausible parameter sets for the TLFs. In this step, we randomly generated several samples of TLF distributions, varied the parameters without any physical rationale, and compared the reproducibility of the key features. We performed this step based on the criterion that the non-monotonicity of frequency shift. Third, we executed gate simulations to validate the improvement of the fidelity with an increase in temperature. Lastly, we discuss the probable source of the TLFs, which can be inferred from the obtained parameter sets.

II. SIMULATION MODELS

Fig.1 depicts the device structure assumed in this study, where the electrons are confined within a quantum dot formed at the

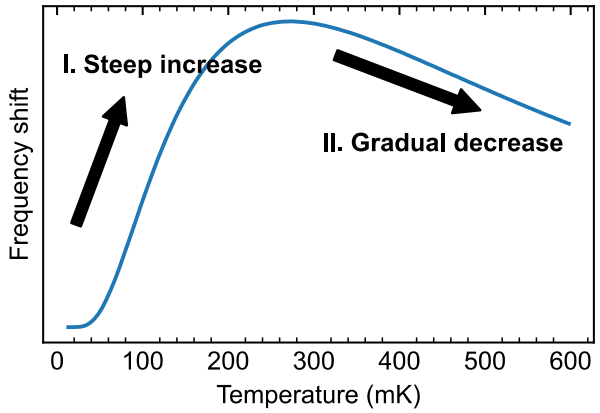

FIGURE 2. Typical experimentally observed temperature dependence of f_q shifts. As indicated by arrows, the frequency shift exhibits steep increase in low temperature region (200 mK) and gradual decrease at higher temperatures (200 mK).

Si/SiGe double heterostructure. Their spins were controlled using microwaves, which was enabled by the magnetic gradient induced by a Co micromagnet. Additionally, TLFs, which produce the charge noise, are assumed to be located at the semiconductor/oxide interface [15], [23].

In such device structures, experiments have demonstrated temperature-dependent f_q shifts that exhibit a distinctive nonmonotonic behavior. This was characterized by a sharp increase in the low temperature region, followed by a gradual decrease at higher temperatures (Fig. 2) [14]. These shifts have been attributed to the temperature dependence of TLF dynamics in some theoretical analyses [13], [16]. However, a comprehensive analysis of this phenomenon, which also accounts for microwave-induced heating during spin control, has not yet been performed. In this section, we present the model that incorporates both the temperature variation due to microwave heating and the Larmor frequency shift induced by the thermal fluctuations of the TLFs, which serve as the foundation for subsequent simulations.

A. f_q SHIFT BY MICROWAVE HEATING

To simulate the experimentally observed temperature variations induced by the microwave pulses, we established a model incorporating both microwave heating and dilution refrigerator cooling. We then fit the model parameters into the experimental data [14].

Silicon qubit devices are typically installed in a dilution refrigerator. This refrigerator maintains a cryogenic environment, which typically ranges from 10 mK to 1 K, to protect the electron spin from thermal noise. However, the temperature of the device increases under the application of microwave signals for qubit operations, which causes f_q shifts. The circular points in Fig. 3 represent the frequency shifts for different pulse durations that were experimentally observed at four base temperatures [14]. The trend of higher base temperatures exhibiting more stable frequencies across varying pulse durations indicates that the temperature variations are less affected by pulse-induced heating at elevated temperatures. This behavior can be attributed to the increased cooling power and heat capacity at higher temperatures. To incorporate these experimental observations, we describe the temperature variation as follows:

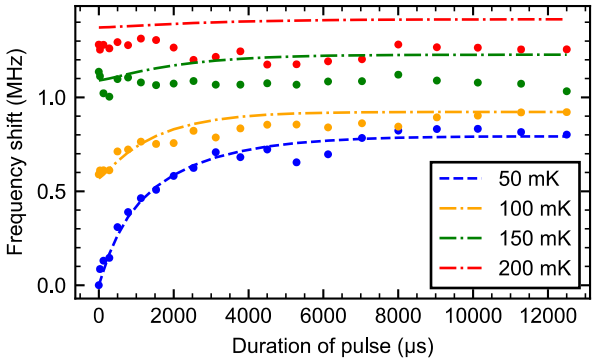

FIGURE 3. Measured f_q shifts as a function of pulse duration at base temperatures of 50, 100, 150, 200 mK (circle points). The blue dashed line represents fitting curve for 50 mK while the dash-dotted lines show the predicted frequency shifts for 100, 150 and 200 mK, calculated using the temperature variation model using the parameters obtained from the fitting for 50 mK. Here, shifts refer to deviations from the f_q at 50 mK prior to the application of the pulse.

$$\frac{dT\,(t)}{dt} = \frac{W_{\text{Joule}}\,(E_{\text{ac}}(t)) - W_{\text{cool}}\,(T\,(t))}{C\,(T\,(t))}, \tag{1}$$

where $T(t)$ denotes the temperature at time t, W_{Joule} denotes the Joule heating power from the applied microwave field with amplitude E_{ac}, W_{cool} denotes the cooling power of the dilution refrigerator, and C denotes the heating capacity of the device. Here, both W_{cool} and C are assumed to be temperature-dependent. To simulate the temperature dependence of the gate fidelity for arbitrary microwave pulse shapes, we fitted the parameters governing the Joule heating, W_{Joule}, contribution induced by the microwave field with the amplitude, $E_{\text{ac}}(t)$, temperature dependence of cooling power, $W_{\text{cool}}(T)$, and heat capacity, $C(T)$. The temperature dependence of the frequency shift Δf_q is fitted to the following model using the experimental data for the Q1 qubit reported in Undseth et al [14]:

$$\Delta f_q\,(T) = \langle s_+\rangle\,(T) f_+ + \langle s_-\rangle\,(T) f_-, \tag{2}$$

$$\langle s_\pm\rangle\,(T) = \pm\frac{1}{e^{-\mu_\pm/T}+1} \mp \frac{1}{e^{(\Delta E_\pm-\mu_\pm)/T}+1}, \tag{3}$$

where $f_\pm$, $\mu_\pm$, and $\Delta E_\pm$ denote the fitting parameters. We combined Eqs. (1), (2) and (3) to model the response of the Δf_q to the applied pulse and its dependence on the pulse duration. The detailed functional forms of these dependencies, frequency shift model, and fitting procedures have been provided in Appendix A.

The blue dashed line in Fig. 3 represents the result of fitting Eq. (1) to the experimental data at a base temperature of 50 mK [14]. The parameters obtained as a result were then used to predict the frequency shift at other base temperatures, as indicated by the dash-dotted lines. The blue line successfully captures the experimental trend, wherein

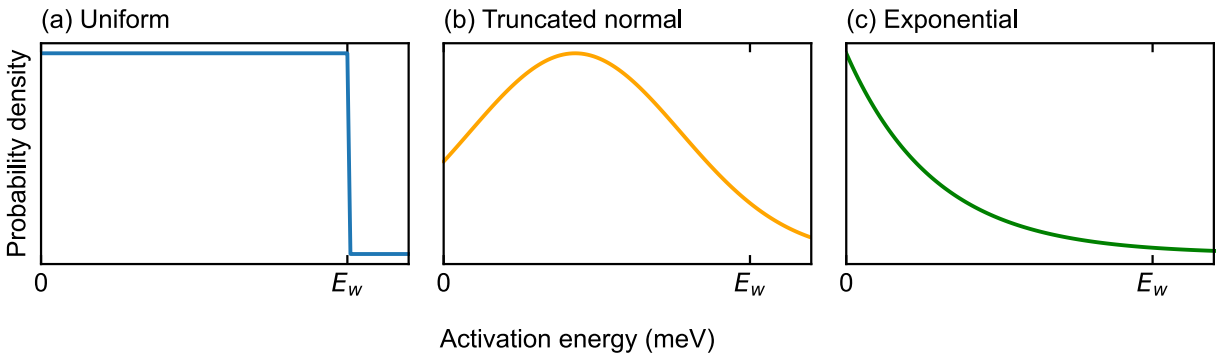

FIGURE 4. Three types of E_A distributions considered in this study: (a) uniform, (b) truncated normal, and (c) exponential. These distributions are used to model the statistical variation of activation energies among thermally fluctuating TLFs.

the frequency shifts increase with pulse duration, particularly in the low-temperature region, as indicated by the blue data points. In addition, the deviations of the dash-dotted lines from the experimental results vary based on the base temperature. For 100 mK, the fitted model effectively captured the overall shift across various pulse durations. For 150 mK and 200 mK, frequency shifts are roughly invariant within the range of experiments, which qualitatively corresponds with experimental results. Conversely, there were deviations between the predicted and measured frequency shifts. These discrepancies arise from long-term fluctuations in the qubit frequency, which were not considered in this fitting process. In the actual experiments, measurements at different temperatures are performed at separate times, leading to random variations in the baseline (offset) of f_q. This offset tends to become larger as the temporal separation between measurements increases. Indeed, as shown in Fig. 3, the 200 mK data already exhibits a noticeable deviation in the offset relative to the 50 mK reference point. As explained in Section II-B, in the latter simulations we consider random f_q fluctuations; the qualitative agreement of the f_q shifts should therefore not be significant within the scope of this study.

B. TLF AND CHARGE NOISE

Charge noise is one of the primary sources of intrinsic noise in the silicon qubit systems. Experiments conducted on silicon devices have indicated that the charge noise affects the Larmor frequency and exhibits a power spectral density (PSD) with a $1/f$ dependence [15], [24], [25], [26], [27]. This behavior can be modeled as a superposition of the electric fluctuations generated by TLFs [28], [29].

An ensemble of TLF can reproduce the temperature dependence of the f_q shift [16]. Here, we assume that the dipole TLF exists in one of two states, denoted by $\pm$, which induces a frequency shift of $\pm\Delta f$ and these states exhibit thermal fluctuation. Under this assumption, the greater the thermal fluctuations, the more rapid the convergence of the finite time average frequency shift Δf to zero within the measurement time. Therefore, an ensemble of TLF can cause temperature-dependent non-monotonic f_q shifts.

We aimed to evaluate the capability of the TLF-based model to reproduce the experimentally observed improvement in gate fidelity at 200 mK. To this end, we computed the gate fidelities using gate-level simulations incorporating the fitted temperature variation model (Section II-A) and the frequency shift model based on the TLF dynamics described below. We present the model used to characterize the thermal fluctuations of the TLFs and describe the approach employed to account for their stochastic variations.

The temperature dependence of mean transition time for TLF τ is given as follows:

$$\tau\,(T) = \tau_{\mathrm{p}}\,(T)\exp\left(\frac{E_{\mathrm{A}}}{k_{\mathrm{B}}T}\right), \tag{4}$$

where the prefactor $\tau_{\mathrm{p}}(T)$ denotes the minimum transition time, E_{A} denotes the activation energy, and k_{B} denotes the Boltzmann constant. Here, we assume that the prefactor exhibits temperature dependence, which can be expressed as follows:

$$\tau_{\mathrm{p}}\,(T) \propto T^{\beta}. \tag{5}$$

For example, the case of $\beta = 0$ corresponds to the Arrhenius equation, $\beta = -1$ corresponds to the Eyring–Polanyi equation, and $\beta = -2$ corresponds to the expression for trap generation-recombination processes (see Section IV-C). According to Eq. (4), the transition times of TLFs with low E_{A} converge to τ_{p} at low temperatures, whereas those with high E_{A} converge at higher temperatures.

Based on the mean transition time, the transition probability of the TLF within a time interval Δt is given by

$$p_{\mathrm{s}}\,(\Delta t) = \frac{1}{2}\left(1 - e^{-\frac{2\Delta t}{\tau}}\right), \tag{6}$$

where τ denotes the temperature-dependent mean transition time from Eq. (4). Therefore, the average charge of the dipole TLF over measurement time t_{m} is expressed as follows:

$$\langle\delta q\rangle\,(t_{\mathrm{m}}) = \delta q\,(0)\exp\left(-\frac{2t_{\mathrm{m}}}{\tau}\right), \tag{7}$$

where $\delta q(0)$ denotes the initial state of the TLF. δq ranges from $-e$ to $+e$. The f_q shift averaged over a given measurement time and initial state can be calculated using Eqs. (4), (6), and (7).

The frequency shift was modeled by considering the displacement caused by each TLF using the Coulomb force and magnetic field gradient within the quantum dot. The detailed expressions for the frequency shift incorporating these effects are provided in Appendix B.

III. SIMULATION METHODS

A. TLF DISTRIBUTION

The physical origin of TLFs is uncertain, due to which their properties, including the activation energy distribution and spatial distribution also remain unclear. Therefore, we first prepared a wide range of possible TLF realizations sampled from several characteristic parameter settings and then determined the resulting temperature dependence of f_q shift and gate fidelity. Subsequently, we analyzed these results to determine the origin of the TLFs. To this end, we divided the TLF realizations into two categories based on whether they could reproduce the experimentally observed non-monotonicity (see Fig. 2). The criteria are defined as follows: (i) the peak absolute value of the frequency shift exceeds 0.4 MHz, (ii) the peak occurs within the temperature range of 100–300 mK, and (iii) the absolute value of frequency shift at 600 mK is less than the peak value, but greater than half this value. We then used subsets of the TLF realizations in each category in gate-level simulations to evaluate the temperature dependence of the gate fidelities.

When preparing the TLF distributions, we considered variations in both the spatial location and the intrinsic characteristics of each TLF. For the spatial distribution, each TLF was assumed to be randomly placed on grid points at the semiconductor/oxide interface with a spacing of 1 nm, within a circular region centered at the qubit position and having a radius of 100 nm. The distance between the interface and the plane in which the quantum dot is formed was set to 30 nm.

For the intrinsic parameters that determine the temperature-dependent behavior of each TLF, we considered several parameter settings. The range was chosen so that the associated TLFs have activation energies that allow transitions within the low-temperature range relevant to this study (20 mK to several hundred mK). In addition, the characteristic time scale must be comparable to the gate duration; otherwise, if the temperature is sufficiently high relative to the activation energy, the fluctuation becomes too fast to affect the qubit frequency and is averaged out within each gate operation. The range of $\tau 0$ was determined based on this requirement. Consequently, we set the parameter settings as follows: (i) three E_A distributions depicted in Fig. 4, i.e., uniform, truncated normal, and exponential distributions, (ii) three values of energy distribution width $E_w \in \{1.5, 3.0, 4.5\}$ meV, (iii) three values of the minimum transition time at 20 mK $\tau_0 \in \{10^{-12}, 10^{-9}, 10^{-6}\}$ s, and (iv) four values of exponent $\beta \in \{-2, -1, 0, 1\}$ in the prefactor $\tau_p(T)$ (see Eq. (5)). This presents a total of 108 unique parameter settings. For each setting, 5,000 different TLF realizations were generated. Additionally, the number of TLF was set to $10\times$ (E_W/1 meV), corresponding to TLF density values of 4.77×10^{10} cm^{-2}, 9.55×10^{10} cm^{-2} and 1.43×10^{11} cm^{-2}. Note that although the energy width, E_w, is defined as the upper limit of the uniform distribution, the shape of the truncated normal and exponential distribution was determined to match the variance of all the distributions. In addition, when sampling the E_A, a truncated normal distribution represents a normal distribution that is limited to positive values and excludes negative values.

B. GATE FIDELITY

We evaluated the gate fidelity of the X gate under temperature-dependent charge noise. In the proposed model, the Hamiltonian governing electron spin dynamics is given as follows:

$$H(t) = \frac{1}{2} f_{\mathrm{Rabi}}(t)\,\sigma_x + \frac{1}{2}\left\{f_q + \delta f_q(t)\right\}\sigma_z, \tag{8}$$

where σ_x and σ_z denote the Pauli matrices, $f_{\mathrm{Rabi}}(t)$ denotes the time-dependent Rabi frequency determined by the microwave amplitude E_{ac}(t), and $\delta f_q(t)$ denotes the calculated temperature-dependent f_q shift. Subsequently, we obtained the unitary time-evolution operator, U, corresponding to the quantum gate operation, by numerically integrating this Hamiltonian into the rotating frame, as described in

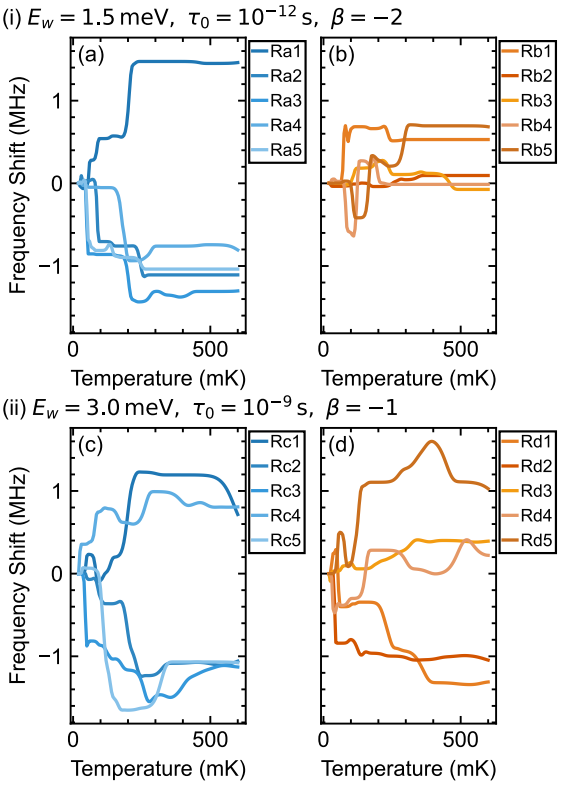

FIGURE 5. Five samples of simulated f_q shifts obtained from different realizations of TLF distribution (labeled Ra1-Ra5, etc.) are shown in each panel. All simulations employ the exponential energy distribution, but different parameter settings are used in cases (i) and (ii). Panels (a) and (c) present realizations that satisfy the non-monotonic frequency-shift behavior observed in experiments, whereas panels (b) and (d) show realizations that do not.

Appendix C. Here, we did not include any energy relaxation processes in the simulation. Thus, the only decoherence mechanism implicitly captured in this model arises from fluctuations in the qubit frequency, which lead to pure dephasing. No additional stochastic dephasing or relaxation channels were incorporated.

The gate fidelity of each execution is evaluated by the average gate fidelity, F_g, which is defined as follows [30]:

$$F_g = \frac{|\mathrm{tr}\,(\sigma_x U)|^2 + 2}{6}, \tag{9}$$

where σ_x denotes the Pauli matrix representing the X gate and U denotes the simulated quantum gate matrix.

Based on the model described above, we first estimated the initial reference frequency, $f_q + \delta f_q(0)$, of the rotating frame based on the mean frequency shift obtained from 10 ms measurements using Eq. (7) for each parameter configuration. We then simulated 1,000 executions of the X gate and reported the mean F_g. The temperature and TLF states were reset to their initial states after every 100 executions to prevent bias toward high-temperature cases. This corresponds to approximately 10 μs of accumulated microwave driving which is consistent with the "tens-of-microseconds" microwave load roughly estimated for randomized benchmarking experiments [14]. The base temperature was swept from 20 to 400 mK in increments of 20 mK. We used a Gaussian waveform for the gate control pulse and its amplitude profile was adjusted to implement a gate duration of $t_g = 100$ ns. The interval between successive gate operations was set to 50 ns.

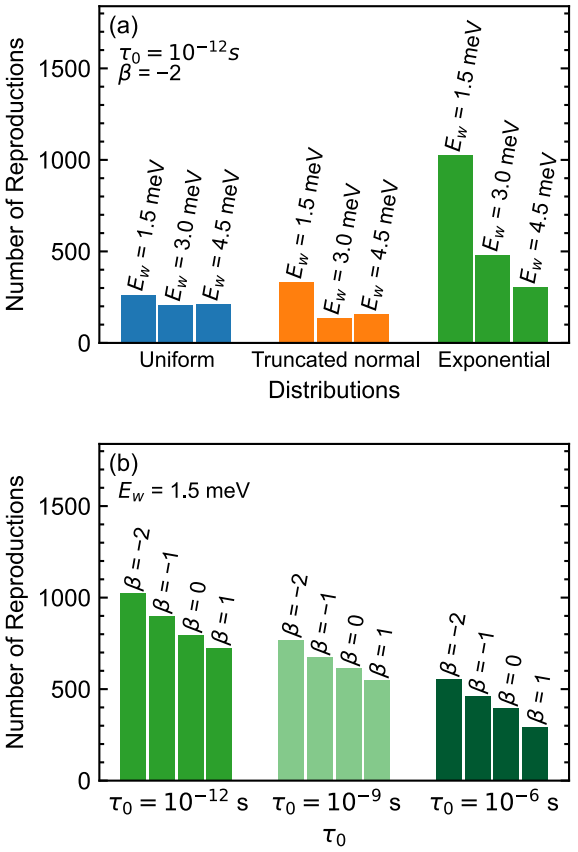

FIGURE 6. Comparisons of the number of successful reproductions of the experimentally observed non-monotonicity: (a) comparison among three different E_A distributions and (b) comparison among different parameter sets in exponential distribution with E_W = 1.5 meV.

IV. RESULTS AND DISCUSSION

A. f_q SHIFT

First, we present the simulated temperature dependence of the f_q shift. Fig. 5 depicts the examples of simulated f_q shifts for two different TLF parameter sets, (i) $\{E_w, \tau_0, \beta\}$={1.5 meV, 10^{-12} s, -2} and (ii) $\{E_w, \tau_0, \beta\}$={3.0 meV, 10^{-9} s, -1}, employing exponential distribution. The graphs on the left (Figs. 5(a) and (c)) depict five curves, each of which exhibited trends similar to the non-monotonicity observed in the experiment based on the aforementioned criteria (see Section III-A). Each curve was obtained from a different spatial TLF distribution. Conversely, the graphs on the right (Figs. 5(b) and (d)) depict five curves that did not exhibit such trends. The TLF characteristics and distribution significantly changed the temperature dependence of the f_q shift.

Subsequently, we aimed to narrow the TLF parameter sets and energetic distributions to determine the most plausible ones in terms of reproducibility. As explained earlier, this strongly depends on the spatial TLF distribution. Therefore, we counted the number of successful cases in all the distributions for each TLF parameter set and energy distribution. The one that reproduced the most frequently was determined to be the most plausible. Fig. 6 depicts the number of TLF distribution that reproduced non-monotonicity under different settings of energy distribution, E_w, τ_0, and β. As shown in Fig. 6(a), The exponential energetic distribution is most likely to reproduce non-monotonicity, and a smaller E_w value is preferred. This is reasonable based on the criteria (ii) of non-monotonicity in this study (see Section III-A). The non-monotonicity of f_q shift exhibits a peak at relatively low temperatures (see Fig. 2). This indicates that more TLFs affected the f_q shift around the temperature of peak and that the number of effective TLFs gradually decreased with an increase in the temperature over this range. According to Eq. (4), this occurs when TLFs with a smaller E_A value are greater than those with a larger E_A value. Therefore, an exponential energetic distribution and a smaller E_W are preferable for reproducing the f_q shift.

Fig. 6(b) depicts the results under different τ_0 and β parameters with a fixed E_w on an exponential energetic distribution. Smaller values of τ_0 and β are preferable as they present a larger change in τ_p with an increase in the temperature within low-temperature range. Thus, TLFs exhibit a greater effect on the f_q shift at lower temperatures. This also helps to satisfy criterion (ii) (see Section III-A).

Not all realizations with the same TLF parameter set reproduced the non-monotonic f_q shift. Essentially, the f_q shift relies heavily on the spatial TLF distribution. It was observed that six qubits simultaneously exhibited similar

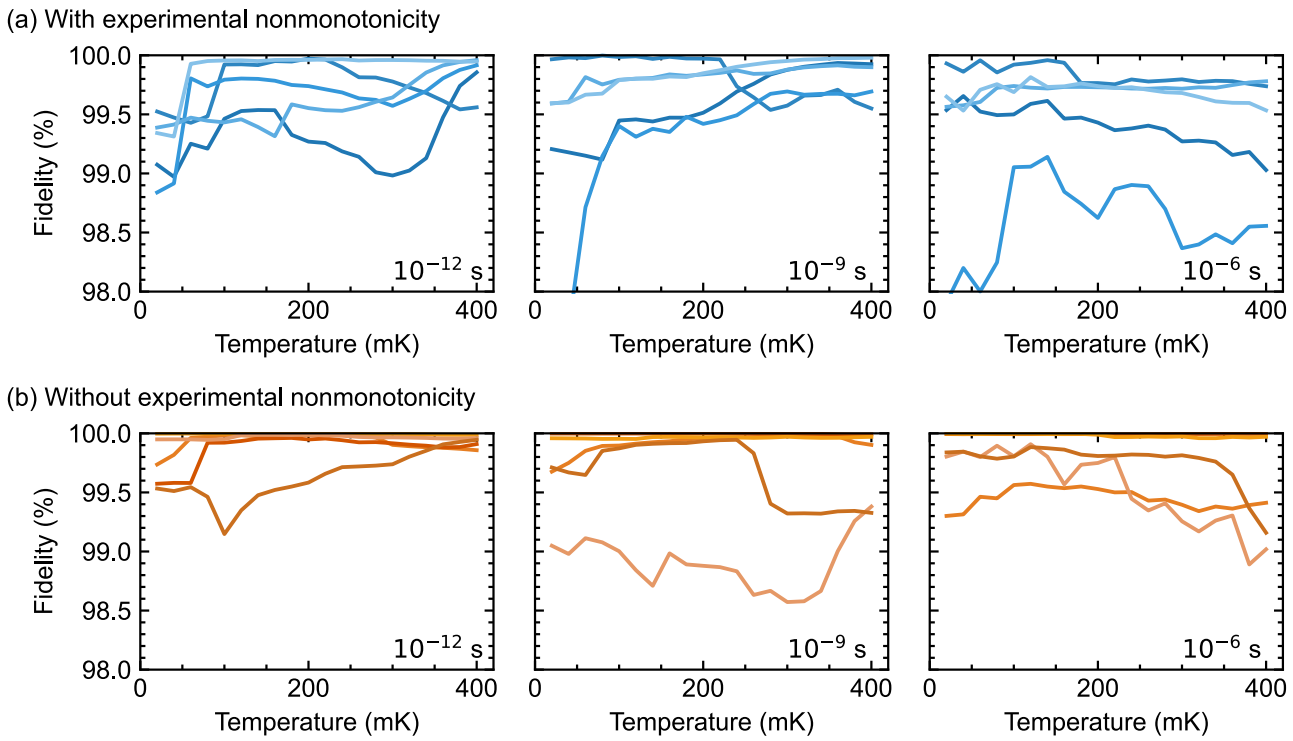

FIGURE 7. Temperature dependence of gate fidelity for five samples corresponding to three different minimum transition time τ_0. (a) exhibits the cases with the TLF realizations that reproduce the f_q non-monotonicity and (b) those that do not. The E_w and β are fixed at 1.5 meV and −2, respectively.

non-monotonicity [14]. This can be attributed to the limitations in the reproducibility of the spatial TLF distribution in our simulation. We randomly placed the TLFs in a physically meaningless manner. Therefore, we did not reproduce the actual TLF distribution in real qubit devices, as it is impossible to determine in detail. Some realizations that we simulated included distributions that were impossible. We believe that it is essential to determine the plausible TLF characteristics using this type of statistical analysis.

B. FIDELITY

In this subsection, we focused on fidelity improvement under operation at higher temperatures. Based on the results discussed in the previous subsection, we employed only plausible exponential distribution. Subsequently, we utilized the TLF realizations sampled from the exponential distribution with 27 different parameter sets. Fig. 7 exhibits example curves of the simulated temperature dependence of gate fidelity for different τ_0 values, with $E_w = 1.5$ meV and $\beta = -2$. Each curve was generated using different realizations with different spatial and energetic TLF distributions. Fig. 7(a) depicts the cases using realizations exhibiting a non-monotonic f_q shift, whereas Fig. 7(b) depicts the cases using realizations that did not exhibit such a shift. Some curves exhibit successful fidelity improvements with an increase in temperature, whereas others do not. It is likely that a shorter τ_0 effectively reproduces the fidelity improvement. In this study, we set the gate duration, t_g, to 100 ns. If the τ_p value becomes shorter than the t_g, the f_q shift averages out during gate operations such that the fidelity is not degraded. Consequently, the fidelity appears to improve with an increase in temperature when the TLF population with a shorter τ_p increases at higher temperatures. However, due to stochastic variations in the activation energy distribution and the number of switching events during a finite gate duration, such fidelity improvement is not guaranteed for every TLF realization, even when $\tau_0 < t_g$.

Subsequently, we statistically considered the TLF realizations based on the reproducibility of the fidelity improvement. We examined the change in gate fidelity with an increase in temperature from 20 to 200 mK. In this time, we performed simulations on 100 TLF realizations for each parameter set, in which we selected 50 realizations that exhibited a non-monotonic f_q shift and 50 realizations that did not. The results were categorized into three types: (i) improved: the fidelity improved by at least 0.1%, (ii) degraded: the fidelity degraded by at least 0.1%, and (iii) not changed: the fidelity changed within ±0.1%. Fig. 8 depicts the statistical results for the cases of realizations that exhibited a non-monotonic f_q shift. It indicates that the cases with smaller values of τ_0 and β are more likely to exhibit the fidelity improvement (type (i), blue bars) in several realizations. This indicates that TLFs with smaller values of τ_0 and β can reproduce the experimentally observed fidelity improvement with an increase in temperature, regardless of their spatial distribution. This is reasonable as a smaller τ_0 indicates that the τ rapidly becomes much shorter than t_g, which reduces the influence of TLF on the gate operation. A smaller β also

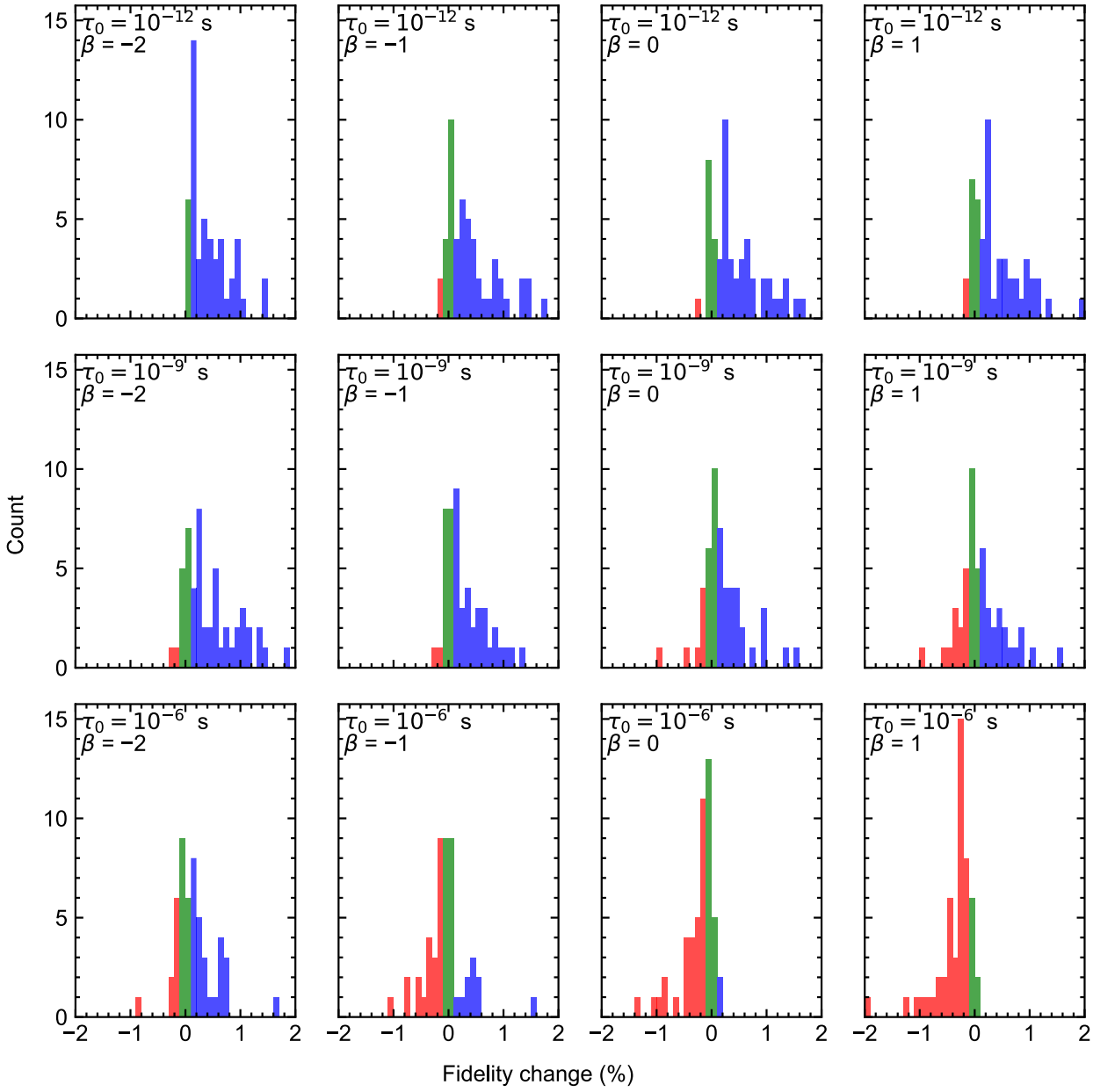

FIGURE 8. Statistical summary of the gate fidelity changes with increasing temperature from 20 to 200 mK, for the cases of the TLF realizations exhibiting the non-monotonic f_q shift, with 12 different parameter settings. Each histogram based on the simulation results using 50 TLF realizations. The histograms are organized by $\tau_0 = 10^{-12}$, 10^{-9} and 10^{-6} s (from top to bottom rows) and $\beta = -2$, -1, 0 and 1 (from left to right columns). Blue, red and green bars correspond to the three categories: (i)improved: the fidelity improved at least 0.1%, (ii)degraded: the fidelity degraded at least 0.1%, and (iii)not changed: the fidelity changed within ±0.1%, respectively.

makes the τ faster with an increase in temperature. Fig. 9 depicts the statistical results for the cases of the realizations that do "not" exhibit a non-monotonic f_q shift. It indicates a similar trend to Fig. 8 regarding the values of τ_0 and β. However, the number of realizations exhibiting a fidelity improvement (type (i), blue bar) was less than that shown in Fig. 8. Furthermore, most realizations did not exhibit fidelity changes (type (iii), green bars). This indicates that a non-monotonic f_q shift, such as shown in Fig. 2, was essential for fidelity improvement.

C. ORIGIN OF TLFS

First, we will summarize the results presented in the previous subsections. From the perspective of the non-monotonic f_q shift and fidelity improvement, we observed that the TLFs exhibiting exponential energetic distribution and smaller E_w, β, and τ_0 values are preferred for reproducing the experiment. In particular, the parameter set $\{E_w, \tau_0, \beta\}=\{1.5\,\text{meV}, 10^{-12}\,\text{s}, -2\}$ was effectively reproduced them regardless of the spatial TLF distribution in our statistical simulation.

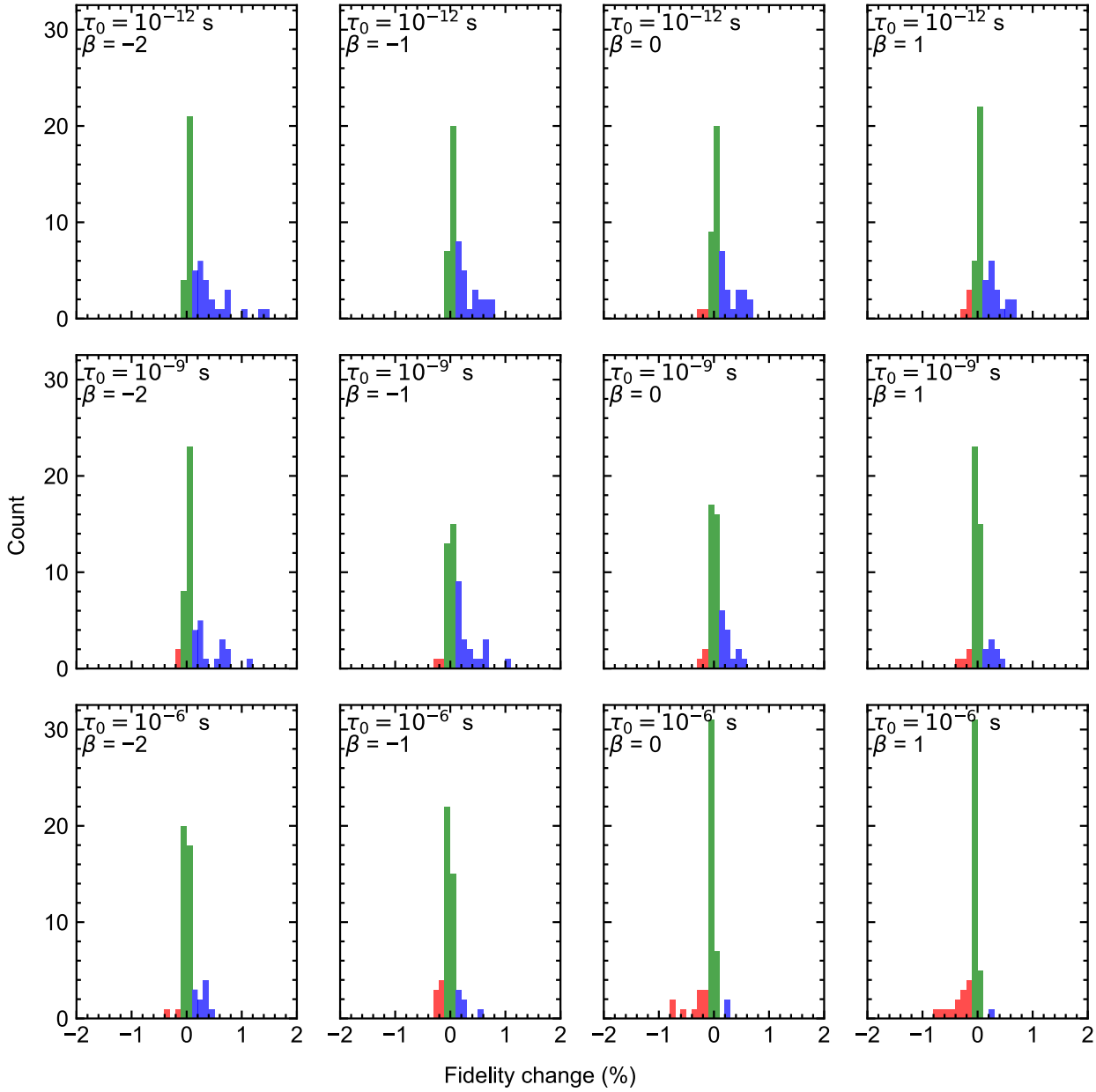

FIGURE 9. Statistical summary like Fig. 8, for the cases of the TLF realizations "not" exhibiting the non-monotonic f_q shift.

In a previous study, some plausible physical origins of TLFs, including dangling bonds at the interface, tunneling atoms, tunneling electrons, and oxygen vacancies were proposed [17]. Some previous simulations have successfully reproduced the experimentally observed frequency shifts using dipole-defect models [13], [16]. In particular, Choi and Joynt. [16] demonstrated that interactions between dipole defects can lead to a non-monotonic temperature dependence. In addition, Champain et al. [13] employed numerical optimization to fit experimental data in hole spins and concluded that an assembly of very small dipoles would be required to explain the observed behavior. These studies provide strong support for the TLF model as a promising framework for understanding temperature-dependent frequency shifts. However, the microscopic physical origin of such defects has not yet been fully clarified.

Driven by this unresolved issue, we conducted a statistical analysis of various TLF properties through systematic manipulation of their temperature dependence, with the objective of narrowing down potential physical origins of TLFs. In addition, we performed gate-level simulations to identify time-dependent TLF characteristics that are most consistent with the experimental observations. Based on the preferred parameter sets obtained from these statistical simulations,

we further narrow down the plausible physical mechanisms underlying TLFs.

Before the beginning of this discussion, we classified them into two categories: atomistic and electronic.

First, we will discuss the atomistic candidates. Typically, for these candidates, it is assumed that a TLF originates from the motion of an atom between the stable and metastable states. The Eyring-Polanyi equation is one approach employed for describing the transition time between these states, based on statistical mechanics, and is expressed as follows [31], [32]:

$$\tau = \kappa \frac{h}{k_B T} \exp\left(\frac{\Delta G^{\ddagger}}{k_B T}\right), \tag{10}$$

where κ denotes the transmission constant, h denotes Planck's constant, $\Delta G^{\ddagger}$ denotes Gibbs energy of activation. Therefore, by comparing Eq. (4) and (10), we can determine $\tau_p(T) \propto 1/T$ ($\beta = -1$ in Eq. (5)). As κ is typically assumed to be 1, the prefactor, τ_p, at $T = 20$ mK is approximately 2×10^{-9} s, which is comparable to the value of $\tau_0 = 1 \times 10^{-9}$ s. This concurs well with our results; however, the problem lies in the E_w value. In this study, we considered the E_w value within a few meV, which corresponds to the discussion of E_A within nearly the same energy range. As discussed previously, a higher E_A is unsuitable for reproducing the f_q shift and fidelity improvement. However, the predicted E_A value for the atomistic candidates is relatively large, within the range of 60 meV to 2 eV [33], [34], [35]. Therefore, the atomistic candidates are unsuitable for the origins of the TLFs, exhibiting f_q shifts and improved fidelity.

Subsequently, we discussed the electronic candidates. The electron transition between the conduction band and the trap level can be determined as the origin of the TLF, which is considered to be the generation-recombination noise in MOSFETs. In this case, the transition time is expressed as follows:

$$\tau = \frac{1}{N_C v_{th} \sigma_t} \exp\left(\frac{E_C - E_T}{k_B T}\right), \tag{11}$$

where N_C denotes the effective electron density of the conduction band edge, v_{th} denotes the thermal velocity of electrons, σ_t denotes the cross-section area of the trap, E_C denotes the energy of the conduction band edge, and E_T denotes the energy of the trap level [36]. As $N_C v_{th} \propto 1/T^2$, this model is comparable to $\beta = -2$. Furthermore, the band edge states are typically considered to exhibit an exponential energetic distribution at the band edge [37], [38], which corresponds to our results. The band edge states were also considered as noise sources in the cryogenic operation of Si MOFETs [23]. When the trap level lies in a band-edge state, the E_A ($= E_C - E_T$ in this case) was observed to be sufficiently low below a few meV [39], [40]. However, it is difficult to determine the τ_p due to uncertainties in the σ_t. If the band-edge states emerge from random potentials [21], [22], [41], the σ_t value increases with a decrease in the E_A value, which presents a τ_p value low enough to reproduce the experimental results even at cryogenic temperatures. For example, when σ_T equals 1×10^{-14} m^2, τ_0 is approximately 2×10^{-8} s.

Another electronic candidate is the inter-trap transition. For example, we can assume in the presence of E'-center-related defects in the SiO_2 gate insulator. These defects can produce dipole-like TLFs owing to the electron distribution around them. However, it is difficult to describe the transition time. We can speculate that their transition time could be sufficiently short to produce an f_q shift and improve the fidelity. We must determine whether these types of defects are energetically distributed exponentially; however, this cannot be evaluated due to the complexity of the situation. At this point, this candidate type cannot be neglected. Therefore, we conclude that the origin of the TLFs is electronic and not atomistic.

Lastly, we would point out that trap-state control methods, such as bias cooling [42], [43], could be useful for controlling the temperature dependence and obtaining more information about the origin of the TLF. Furthermore, in order to experimentally validate our conclusion, it is essential to obtain a better understanding of the electron state at the Si/SiO_2 interface in both the many-electron [44], [45], [46] and few-electron regimes, the latter corresponding to qubit operations.

V. CONCLUSION

In this study, we investigated the temperature dependence of spin qubits implemented in Si/SiGe devices through simulations based on the f_q shift and gate fidelity improvement with an increase in the operation temperature. We performed a statistical analysis to consider the energetic and random spatial TLF distributions. The simulation results indicate that TLFs with an exponential activation energy distribution, short transition times, and steep temperature transitions can effectively reproduce the experimental findings of previous studies. Furthermore, quantum-gate-level simulations demonstrated that fidelity improvement with an increase in the operating temperature occurs when TLF dynamics cause transition times much shorter than the gate times and exhibit a steep transition against temperature. Based on these results, we concluded that electronic processes, such as the transitions between the conduction band and trap states, are plausible origins of TLFs.

APPENDIX A
TEMPERATURE VARIATION MODEL

In this appendix, we present a detailed description of the fitting procedures employed to reproduce the f_q shift as a function of the pulse duration used in this study.

First, we assume the time dependency of each component in Eq. (1). The total Joule heating energy over time interval t is given as follows [47]:

$$E_{Joule} = \int_t dt' \int_V d\mathbf{r} \frac{\sigma(\mathbf{r}) + \omega\epsilon(\mathbf{r})}{2} \left|E_{ac}(t')\right|^2, \tag{12}$$

where V denotes the volume in which the microwave field penetrates, ω denotes the angular frequency of the microwave, and $\sigma(\mathbf{r})$ and $\epsilon(\mathbf{r})$ denote the position-dependent conductive and dielectric losses, respectively. Due to the uncertainty in volume, V, we simplified Eq. (12) as follows:

$$W_{\text{Joule}}(t) = \left(\sigma' + \omega\epsilon'\right)|E_{\text{ac}}(t)|^2, \tag{13}$$

where σ' and ϵ' denote the fitting parameters.

Although the detailed temperature dependence of the cooling power of the refrigerator was not fully characterized, it was predicted to improve with an increase in temperature [14], [48], [49]. To model this behavior, we expressed the cooling power, W_{cool}, as follows:

$$W_{\text{cool}} = \begin{cases} \alpha_{\text{c}} T_0^{\kappa} (T - T_0)^{\gamma}, & T > T_0 \\ 0, & T \leq T_0 \end{cases} \tag{14}$$

where T denotes the electron temperature of the device, T_0 denotes the base temperature of dilution refrigerator, and α_{c}, κ, and γ denote the fitting parameters.

The heat capacity $C(T)$ was modeled using the Debye model, which predicts the cubic dependence on temperature as follows:

$$C(T) = k_{\text{C}} T^3, \tag{15}$$

where k_{C} denotes a fitting parameter.

Combining Eqs. (1), (13), (14), and (15), we established a temperature variation model with six fitting parameters.

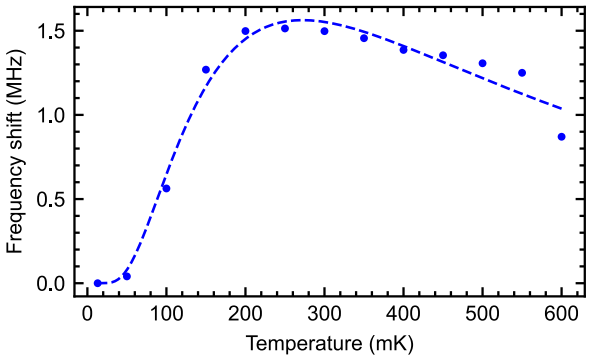

FIGURE 10. Experimental f_{q} shifts (circle markers) [14] and the corresponding fitting curve (dashed line) as a function of dilution refrigerator temperatures.

For this fitting, we require the static temperature dependence of the f_{q}, that does not consider the pulses. This is the case of equilibrium state ($T = T_0$). We then modeled the f_{q} shift as follows (the same expression as presented in Section II-A):

$$\Delta f_q(T) = \langle s_+ \rangle(T) f_+ + \langle s_- \rangle(T) f_-, \tag{16}$$

$$\langle s_\pm \rangle(T) = \pm \frac{1}{e^{-\mu_\pm/T} + 1} \mp \frac{1}{e^{(\Delta E_\pm - \mu_\pm)/T} + 1}, \tag{17}$$

where $f_\pm$, $\mu_\pm$, and Δ E$_\pm$ denote the fitting parameters.

Subsequently, the fitting process is explained. First, the static temperature dependence of f_{q} was fitted using Eqs. (14) and (15). We used the experimental data for the Q1 qubit denoted by Undseth et al. [14], and fitting was performed using the least-squares method. Fig. 10 depicts the fitting result, which captures the overall trend of the f_{q} shift as a function of the temperature.

TABLE 1. Fitting parameters obtained from experimental data describing the relationship between input energy and qubit frequency shift [14].

Parameter	Value
f_+	3.74 MHz
ΔE_+	1528.05 mK
μ_+	881.31 mK
f_-	3.28 MHz
ΔE_-	440.09 mK
μ_-	217.16 mK
γ	0.70
κ	0.80
σ	541.8 J//V^2
ϵ	85.43 J ns/V^2
k_{C}	6.62×10^{-3} J/mK^4
W_{cool}	0.17 J

Subsequently, we constructed the f_{q} shift model as a function of the pulse duration at 50 mK, as shown in Fig. 3. We numerically solved Eq. (1) as a differential equation by combining Eqs. (13)–(15) using the Euler method with a time increment of 0.1 ns. In this process, the parameters were iteratively fitted using the least-squares method. We then obtained a fitting curve for the experimental data at 50 mK as indicated by the blue dashed line in Fig. 3. Subsequently, we generated other curves for different base temperatures using the obtained fitting parameters, as indicated by the dash-dotted lines in Fig. 3.

We manually set parameters γ and κ because it is difficult to simultaneously converge all the parameters. Among several combinations of (γ, κ), we selected the parameters that can provide the best reproduction regarding all the curves depicted in Fig. 3. Table 1 summarizes the final fitting parameters.

APPENDIX B
TLF-INDUCED FREQUENCY SHIFT MODEL

In this appendix, we describe the procedure used to obtain the f_{q} shift from the state of the TLF δq. In the presence of a magnetic gradient due to a micromagnet, the displacement of the confined electrons induced by electric field fluctuations causes an f_{q} shift. When the in-plane magnetic field gradients are $\partial B/\partial x$ and $\partial B/\partial y$, the f_{q} shift is given as: [27]

$$\delta f = \frac{g\mu_B}{h} \frac{e}{m\omega_{\text{c}}^2} \left(\frac{\partial B}{\partial x} \delta E_x + \frac{\partial B}{\partial z} \delta E_y \right), \tag{18}$$

where μ_{B} denotes the Bohr magneton, $\hbar$ denotes the reduced Planck's constant, $\hbar\omega_{\text{c}}$ denotes the confinement energy of the electron, B denotes the z-component of the magnetic field at the quantum dot's position, g denotes the g-factor, and δE_x and δE_y denote the in-plane components of the TLF-induced

TABLE 2. Parameters used in the charge noise simulations. Here, m_0 denotes the free electron mass, and the confinement potential is assumed to be parabolic.

Parameter	Value
$\partial B/\partial x$	0.1 mT/nm
$\partial B/\partial y$	−0.01 mT/nm
g	2
m/m_0	0.19
$\hbar\omega_c$	2 meV

electric field. The z-component is neglected due to strong confinement along the z-direction, which keeps the displacement along this direction small.

In this study, we modeled each TLF as a dipole comprising two oppositely charged entities separated by a short distance. Although the exact physical structure of a TLF remains uncertain, the simulations performed in previous studies reported that dipole configurations are plausible sources of the experimentally observed noise [29], [50].

The electric field $\delta\,\mathbf{E}$ at the quantum dot fluctuated by each TLF possessing δq is given by:

$$\delta\mathbf{E} = \frac{1}{4\pi\epsilon_r\epsilon_0}\left(\frac{\mathbf{r}}{|\mathbf{r}|^3}\delta q - \frac{\mathbf{r}_i'}{|\mathbf{r}_i'|^3}\delta q\right), \tag{19}$$

where $\mathbf{r}$ and $\mathbf{r}$' denote the positions of the two charges forming the dipole from the quantum dot, and $\delta q \in \{-e, e\}$ denotes the dipole state. The distance between the two charges on the dipole was fixed at 1 nm. All the TLFs were placed with the dipole axis parallel to the z-axis. The dielectric constant, ϵ_r, is set to 13 of $Si_{0.7}Ge_{0.3}$, and ϵ_0 denotes the vacuum permittivity. Table 2 summarizes the other parameters used in this work.

APPENDIX C
GATE SIMULATION MODEL

In this appendix, we present a method for quantum gate simulations under the f_q shift.

In the rotating frame defined by the axis, $(f_q + \Delta f_{init})\sigma_z/2$, using the Hamiltonian given in Eq. (8), the unitary evolution during the gate time t_g is approximated as follows:

$$U\,(t+\Delta t) \approx \exp\left[-\frac{i}{\hbar}\left\{\frac{1}{2}f_{\mathrm{Rabi}}\,(t)\,\sigma_x + \frac{1}{2}\left(\Delta f_q - \Delta f_{\mathrm{init}}\right)\sigma_z\right\}\Delta t\right] U(t), \tag{20}$$

where $\Delta t = t_g/N$ and Δf_{init} denotes the initial frequency shift determined by calibration process. In this study, Δf_{init} is evaluated for each TLF realization, for which the initial δq must be estimated. Subsequently, we employed the δq at $t_m = 10$ ms, which was obtained from Eq. (7) as the initial value, in which $\delta q(0)$ was randomly obtained.

The relationship between the microwave amplitude, $E_{ac}(t)$, and the Rabi frequency, $f_{rabi}(t)$, was determined using experimental data as follows [14]:

$$f_{\mathrm{Rabi}}\,(t) = \frac{1.3\ \mathrm{MHz}}{0.2\ \mathrm{V}} E_{\mathrm{ac}}\,(t)\ \mathrm{V}. \tag{21}$$

Here, we assumed that f_{rabi} value increases linearly with E_{ac} [51], [52].

REFERENCES

[1] D. Loss and D. P. DiVincenzo, "Quantum computation with quantum dots," *Phys. Rev. A, Gen. Phys.*, vol. 57, no. 1, pp. 120–126, Jan. 1998, doi: 10.1103/physreva.57.120.

[2] G. Burkard, T. D. Ladd, A. Pan, J. M. Nichol, and J. R. Petta, "Semiconductor spin qubits," *Rev. Modern Phys.*, vol. 95, no. 2, Jun. 2023, Art. no. 025003, doi: 10.1103/revmodphys.95.025003.

[3] K. Takeda, J. Yoneda, T. Otsuka, T. Nakajima, M. R. Delbecq, G. Allison, Y. Hoshi, N. Usami, K. M. Itoh, S. Oda, T. Kodera, and S. Tarucha, "Optimized electrical control of a Si/SiGe spin qubit in the presence of an induced frequency shift," *npj Quantum Inf.*, vol. 4, no. 1, p. 54, Oct. 2018, doi: 10.1038/s41534-018-0105-z.

[4] X. Xue et al., "CMOS-based cryogenic control of silicon quantum circuits," *Nature*, vol. 593, no. 7858, pp. 205–210, May 2021, doi: 10.1038/s41586-021-03469-4.

[5] A. Noiri, K. Takeda, T. Nakajima, T. Kobayashi, A. Sammak, G. Scappucci, and S. Tarucha, "Fast universal quantum gate above the fault-tolerance threshold in silicon," *Nature*, vol. 601, no. 7893, pp. 338–342, Jan. 2022, doi: 10.1038/s41586-021-04182-y.

[6] A. R. Mills, C. R. Guinn, M. J. Gullans, A. J. Sigillito, M. M. Feldman, E. Nielsen, and J. R. Petta, "Two-qubit silicon quantum processor with operation fidelity exceeding 99%," *Sci. Adv.*, vol. 8, no. 14, Apr. 2022, Art. no. eabn5130, doi: 10.1126/sciadv.abn5130.

[7] S. G. J. Philips, M. T. Mądzik, S. V. Amitonov, S. L. De Snoo, M. Russ, N. Kalhor, C. Volk, W. I. L. Lawrie, D. Brousse, L. Tryputen, B. P. Wuetz, A. Sammak, M. Veldhorst, G. Scappucci, and L. M. K. Vandersypen, "Universal control of a six-qubit quantum processor in silicon," *Nature*, vol. 609, no. 7929, pp. 919–924, Sep. 2022, doi: 10.1038/s41586-022-05117-x.

[8] J. Y. Huang et al., "High-fidelity spin qubit operation and algorithmic initialization above 1 K," *Nature*, vol. 627, no. 8005, pp. 772–777, Mar. 2024, doi: 10.1038/s41586-024-07160-2.

[9] R. Raussendorf and J. Harrington, "Fault-tolerant quantum computation with high threshold in two dimensions," *Phys. Rev. Lett.*, vol. 98, no. 19, May 2007, Art. no. 190504, doi: 10.1103/physrevlett.98.190504.

[10] A. M. Stephens, "Fault-tolerant thresholds for quantum error correction with the surface code," *Phys. Rev. A, Gen. Phys.*, vol. 89, no. 2, Feb. 2014, Art. no. 022321, doi: 10.1103/physreva.89.022321.

[11] T. F. Watson, S. G. J. Philips, E. Kawakami, D. R. Ward, P. Scarlino, M. Veldhorst, D. E. Savage, M. G. Lagally, M. Friesen, S. N. Coppersmith, M. A. Eriksson, and L. M. K. Vandersypen, "A programmable two-qubit quantum processor in silicon," *Nature*, vol. 555, no. 7698, pp. 633–637, Mar. 2018, doi: 10.1038/nature25766.

[12] A. M. J. Zwerver et al., "Qubits made by advanced semiconductor manufacturing," *Nature Electron.*, vol. 5, no. 3, pp. 184–190, Mar. 2022, doi: 10.1038/s41928-022-00727-9.

[13] V. Champain, G. Boschetto, H. Niebojewski, B. Bertrand, L. Mauro, M. Bassi, V. Schmitt, X. Jehl, S. Zihlmann, R. Maurand, Y.-M. Niquet, C. B. Winkelmann, S. De Franceschi, B. Martinez, and B. Brun, "A heat-resilient hole spin qubit in silicon," 2025, *arXiv:2509.15823*.

[14] B. Undseth, O. Pietx-Casas, E. Raymenants, M. Mehmandoost, M. T. Mądzik, S. G. J. Philips, S. L. De Snoo, D. J. Michalak, S. V. Amitonov, L. Tryputen, B. P. Wuetz, V. Fezzi, D. D. Esposti, A. Sammak, G. Scappucci, and L. M. K. Vandersypen, "Hotter is easier: Unexpected temperature dependence of spin qubit frequencies," *Phys. Rev. X*, vol. 13, no. 4, Oct. 2023, Art. no. 041015, doi: 10.1103/physrevx.13.041015.

[15] E. J. Connors, J. Nelson, H. Qiao, L. F. Edge, and J. M. Nichol, "Low-frequency charge noise in Si/SiGe quantum dots," *Phys. Rev. B, Condens. Matter*, vol. 100, no. 16, Oct. 2019, Art. no. 165305, doi: 10.1103/physrevb.100.165305.

[16] Y. Choi and R. Joynt, "Interacting random-field dipole defect model for heating in semiconductor-based qubit devices," *Phys. Rev. Res.*, vol. 6, no. 1, Feb. 2024, Art. no. 013168, doi: 10.1103/physrevresearch.6.013168.

[17] C. Müller, J. H. Cole, and J. Lisenfeld, "Towards understanding two-level-systems in amorphous solids: Insights from quantum circuits," *Rep. Prog. Phys.*, vol. 82, no. 12, Oct. 2019, Art. no. 124501, doi: 10.1088/1361-6633/ab3a7e.

[18] D. M. Fleetwood, H. D. Xiong, Z.-Y. Lu, C. J. Nicklaw, J. A. Felix, R. D. Schrimpf, and S. T. Pantelides, "Unified model of hole trapping, 1/f noise, and thermally stimulated current in MOS devices," *IEEE Trans. Nucl. Sci.*, vol. 49, no. 6, pp. 2674–2683, Dec. 2002, doi: 10.1109/TNS.2002.805407.

[19] W. Goes, Y. Wimmer, A.-M. El-Sayed, G. Rzepa, M. Jech, A. L. Shluger, and T. Grasser, "Identification of oxide defects in semiconductor devices: A systematic approach linking DFT to rate equations and experimental evidence," *Microelectron. Rel.*, vol. 87, pp. 286–320, Aug. 2018, doi: 10.1016/j.microrel.2017.12.021.

[20] M. Cowie, P. C. Constantinou, N. J. Curson, T. J. Z. Stock, and P. Grütter, "Spatially resolved random telegraph fluctuations of a single trap at the Si/SiO_2 interface," *Proc. Nat. Acad. Sci. USA*, vol. 121, no. 44, Oct. 2024, Art. no. 2404456121, doi: 10.1073/pnas.2404456121.

[21] E. O. Kane, "Thomas-Fermi approach to impure semiconductor band structure," *Phys. Rev.*, vol. 131, no. 1, pp. 79–88, Jul. 1963, doi: 10.1103/physrev.131.79.

[22] B. I. Halperin and M. Lax, "Impurity-band tails in the high-density limit. I. Minimum counting methods," *Phys. Rev.*, vol. 148, no. 2, pp. 722–740, Aug. 1966, doi: 10.1103/physrev.148.722.

[23] H. Oka, T. Inaba, S. Shitakata, K. Kato, S. Iizuka, H. Asai, H. Fuketa, and T. Mori, "Origin of low-frequency noise in Si n-MOSFET at cryogenic temperatures: The effect of interface quality," *IEEE Access*, vol. 11, pp. 121567–121573, 2023, doi: 10.1109/ACCESS.2023.3327731.

[24] J. Yoneda, K. Takeda, T. Otsuka, T. Nakajima, M. R. Delbecq, G. Allison, T. Honda, T. Kodera, S. Oda, Y. Hoshi, N. Usami, K. M. Itoh, and S. Tarucha, "A quantum-dot spin qubit with coherence limited by charge noise and fidelity higher than 99.9%," *Nature Nanotechnol.*, vol. 13, no. 2, pp. 102–106, Feb. 2018, doi: 10.1038/s41565-017-0014-x.

[25] E. J. Connors, J. Nelson, L. F. Edge, and J. M. Nichol, "Charge-noise spectroscopy of Si/SiGe quantum dots via dynamically-decoupled exchange oscillations," *Nature Commun.*, vol. 13, no. 1, p. 940, Feb. 2022, doi: 10.1038/s41467-022-28519-x.

[26] J. Yoneda, J. S. Rojas-Arias, P. Stano, K. Takeda, A. Noiri, T. Nakajima, D. Loss, and S. Tarucha, "Noise-correlation spectrum for a pair of spin qubits in silicon," *Nature Phys.*, vol. 19, no. 12, pp. 1793–1798, Dec. 2023, doi: 10.1038/s41567-023-02238-6.

[27] J. S. Rojas-Arias, A. Noiri, P. Stano, T. Nakajima, J. Yoneda, K. Takeda, T. Kobayashi, A. Sammak, G. Scappucci, D. Loss, and S. Tarucha, "Spatial noise correlations beyond nearest neighbors in ^{28}Si/ Si-Ge spin qubits," *Phys. Rev. Appl.*, vol. 20, no. 5, Nov. 2023, Art. no. 054024, doi: 10.1103/physrevapplied.20.054024.

[28] U. Güngördü and J. P. Kestner, "Indications of a soft cutoff frequency in the charge noise of a Si/SiGe quantum dot spin qubit," *Phys. Rev. B, Condens. Matter*, vol. 99, no. 8, Feb. 2019, Art. no. 081301, doi: 10.1103/physrevb.99.081301.

[29] M. M. E. K. Shehata, G. Simion, R. Li, F. A. Mohiyaddin, D. Wan, M. Mongillo, B. Govoreanu, I. Radu, K. De Greve, and P. Van Dorpe, "Modeling semiconductor spin qubits and their charge noise environment for quantum gate fidelity estimation," *Phys. Rev. B, Condens. Matter*, vol. 108, no. 4, Jul. 2023, Art. no. 045305, doi: 10.1103/physrevb.108.045305.

[30] M. A. Nielsen, "A simple formula for the average gate fidelity of a quantum dynamical operation," *Phys. Lett. A*, vol. 303, no. 4, pp. 249–252, Oct. 2002, doi: 10.1016/s0375-9601(02)01272-0.

[31] H. Eyring, "The activated complex in chemical reactions," *J. Chem. Phys.*, vol. 3, no. 2, pp. 107–115, Feb. 1935, doi: 10.1063/1.1749604.

[32] M. G. Evans and M. Polanyi, "Some applications of the transition state method to the calculation of reaction velocities, especially in solution," *Trans. Faraday Soc.*, vol. 31, pp. 875–894, Jan. 1935, doi: 10.1039/tf9353100875.

[33] R. Biswas and Y.-P. Li, "Hydrogen flip model for light-induced changes of amorphous silicon," *Phys. Rev. Lett.*, vol. 82, no. 12, pp. 2512–2515, Mar. 1999, doi: 10.1103/physrevlett.82.2512.

[34] A.-M. El-Sayed, M. B. Watkins, T. Grasser, V. V. Afanas'ev, and A. L. Shluger, "Hydrogen-induced rupture of strained Si–O bonds in amorphous silicon dioxide," *Phys. Rev. Lett.*, vol. 114, no. 11, Mar. 2015, Art. no. 115503, doi: 10.1103/physrevlett.114.115503.

[35] T. Damart and D. Rodney, "Atomistic study of two-level systems in amorphous silica," *Phys. Rev. B, Condens. Matter*, vol. 97, no. 1, Jan. 2018, Art. no. 014201, doi: 10.1103/physrevb.97.014201.

[36] D. C. Murray, A. G. R. Evans, and J. C. Carter, "Shallow defects responsible for GR noise in MOSFETs," *IEEE Trans. Electron Devices*, vol. 38, no. 2, pp. 407–416, Feb. 1991, doi: 10.1109/16.69924.

[37] H. Hasegawa and T. Sawada, "On the distribution and properties of interface states at compound semiconductor-insulator interfaces," *Surf. Sci.*, vol. 98, nos. 1–3, pp. 597–598, Aug. 1980, doi: 10.1016/0039-6028(80)90539-7.

[38] N. M. Johnson, D. K. Biegelsen, M. D. Moyer, S. T. Chang, E. H. Poindexter, and P. J. Caplan, "Characteristic electronic defects at the $Si-SiO_2$ interface," *Appl. Phys. Lett.*, vol. 43, no. 6, pp. 563–565, Sep. 1983, doi: 10.1063/1.94420.

[39] C. Spence, B. Cardoso Paz, V. Michal, E. Chanrion, D. J. Niegemann, B. Jadot, P.-A. Mortemousque, B. Klemt, V. Thiney, B. Bertrand, L. Hutin, C. Bäuerle, M. Vinet, Y.-M. Niquet, T. Meunier, and M. Urdampilleta, "Probing low-frequency charge noise in few-electron CMOS quantum dots," *Phys. Rev. Appl.*, vol. 19, no. 4, Apr. 2023, Art. no. 044010, doi: 10.1103/physrevapplied.19.044010.

[40] K. Ohmori et al., "Characterization of very shallow states in cryogenic MOSFETs by wideband noise spectroscopy," *TechRxiv*, Apr. 2024, doi: 10.36227/techrxiv.171440863.39634816/v1.

[41] N. Mori, "Effect of random potential on two-dimensional electronic states," *Jpn. J. Appl. Phys.*, vol. 64, no. 1, Jan. 2025, Art. no. 01SP14, doi: 10.35848/1347-4065/ad9c85.

[42] J. Ferrero, T. Koch, S. Vogel, D. Schroller, V. Adam, R. Xue, I. Seidler, L. R. Schreiber, H. Bluhm, and W. Wernsdorfer, "Noise reduction by bias cooling in gated Si/Si_xGe_{1-x} quantum dots," *Appl. Phys. Lett.*, vol. 124, no. 20, May 2024, Art. no. 204002, doi: 10.1063/5.0206632.

[43] L. K. Diebel, L. G. Zinkl, A. Hötzinger, F. Reichmann, M. Lisker, Y. Yamamoto, and D. Bougeard, "Impact of biased cooling on the operation of undoped silicon quantum well field-effect devices," *AIP Adv.*, vol. 15, no. 3, Mar. 2025, Art. no. 035301, doi: 10.1063/5.0250968.

[44] S. Chattopadhyay, K. S. K. Kwa, S. H. Olsen, L. S. Driscoll, and A. G. O. Neill, "C–V characterization of strained Si/SiGe multiple heterojunction capacitors as a tool for heterojunction MOSFET channel design," *Semicond. Sci. Technol.*, vol. 18, no. 8, pp. 738–744, Jul. 2003, doi: 10.1088/0268-1242/18/8/304.

[45] T. M. Lu, C.-H. Lee, S.-H. Huang, D. C. Tsui, and C. W. Liu, "Upper limit of two-dimensional electron density in enhancement-mode Si/SiGe heterostructure field-effect transistors," *Appl. Phys. Lett.*, vol. 99, no. 15, Oct. 2011, Art. no. 153510, doi: 10.1063/1.3652909.

[46] F. Stampfl, C. Godfrin, S. Kubicek, S. Baudot, B. Raes, K. De Greve, A. Grill, and M. Waltl, "CV characterization of Si/SiGe heterostructures at cryo temperatures," in *Proc. IEEE Int. Rel. Phys. Symp. (IRPS)*, Monterey, CA, USA, Mar. 2025, pp. 1–5, doi: 10.1109/IRPS48204.2025.10982705.

[47] D. M. Pozar, *Microwave Engineering*, 4th ed., Hoboken, NJ, USA: Wiley, 2012.

[48] M. A. Green, "The cost of coolers for cooling superconducting devices at temperatures at 4.2 K, 20 K, 40 K and 77 K," *Proc. IOP Conf. Ser. Mater. Sci. Eng.*, vol. 101, Jan. 2015, Art. no. 012001, doi: 10.1088/1757-899x/101/1/012001.

[49] *XLDsl Dilution Refrigerator Measurement System*. Accessed: Oct. 23, 2025. [Online]. Available: https://bluefors.com/products/dilution-refrigerator-measurement-systems/xldsl-dilution-refrigerator-measurement-system/

[50] M. Kępa, Ł. Cywiński, and J. A. Krzywda, "Correlations of spin splitting and orbital fluctuations due to 1/f charge noise in the Si/SiGe quantum dot," *Appl. Phys. Lett.*, vol. 123, no. 3, Jul. 2023, Art. no. 034003, doi: 10.1063/5.0156358.

[51] M. Pioro-Ladrière, T. Obata, Y. Tokura, Y.-S. Shin, T. Kubo, K. Yoshida, T. Taniyama, and S. Tarucha, "Electrically driven single-electron spin resonance in a slanting Zeeman field," *Nature Phys.*, vol. 4, no. 10, pp. 776–779, Oct. 2008, doi: 10.1038/nphys1053.

[52] K. Takeda, J. Kamioka, T. Otsuka, J. Yoneda, T. Nakajima, M. R. Delbecq, S. Amaha, G. Allison, T. Kodera, S. Oda, and S. Tarucha, "A fault-tolerant addressable spin qubit in a natural silicon quantum dot," *Sci. Adv.*, vol. 2, no. 8, Aug. 2016, Art. no. 1600694, doi: 10.1126/sciadv.1600694.

YUDAI SATO received the B.E. degree in electrical engineering from Tokyo University of Science, Tokyo, Japan, in 2024, where he is currently pursuing the M.E. degree in electrical engineering. He is also with the Semiconductor Frontier Research Center (SFRC), National Institute of Advanced Industrial Science and Technology (AIST), as a Research Assistant. His research interests include silicon quantum hardware and qubit control methods.

HIDEHIRO ASAI (Member, IEEE) received the B.S., M.S., and Ph.D. degrees in materials engineering from The University of Tokyo, Tokyo, Japan, in 2004, 2006, and 2009, respectively. He is currently a Senior Researcher with the Semiconductor Frontier Research Center (SFRC), National Institute of Advanced Industrial Science and Technology (AIST), Ibaraki, Japan. His research interests include the numerical design of the Si quantum computer hardware and the cryogenic MOSFET.

TAKAHIRO MORI (Member, IEEE) received the B.S., M.S., and Ph.D. degrees in applied physics from Tohoku University, Sendai, Japan, in 2001, 2003, and 2006, respectively. He is currently the Research Team Leader with the Semiconductor Frontier Research Center (SFRC), National Institute of Advanced Industrial Science and Technology (AIST), Tsukuba, Japan. His research interests include Si quantum computer hardware and leading-edge transistor technologies.

TAKAYUKI KAWAHARA (Life Fellow, IEEE) received the B.S. and M.S. degrees in physics and the Ph.D. degree in electronics from Kyushu University, Fukuoka, Japan, in 1983, 1985, and 1993, respectively.

In 1985, he joined the Central Research Laboratory (CRL), Hitachi Ltd., where he made fundamental contributions to low-power memory technologies. His notable achievements in DRAM circuit research include techniques for low-voltage operation, such as subthreshold-current reduction via gate-source self-reverse biasing, in 1993, and an overdrive sense amplifier scheme with direct sensing. He also pioneered the charge-recycling scheme, reported, in 1993, which has since been widely adopted across various circuits. In the field of flash memory, he and his team developed a 128-Mb chip that employed a bit-line clamped sensing scheme for fast sensing and a high-voltage generator architecture compatible with low-voltage supplies, in 1996. He was a Visiting Researcher with the Electronics Laboratory (LEG), Swiss Federal Institute of Technology, Lausanne (EPFL), from 1997 to 1998. In addition, he led the ultra-low-power System LSI Project at CRL and, in emerging memory and device research, reported the first fully functional 2-Mb STT-RAM prototype chip, in 2007. His team also developed FD-SOI SRAM circuitry featuring back-gate control. Subsequently, he contributed to circuitry development for DNA sequencers, including statistical nanopore systems and fast ISFET arrays. In 2014, he was appointed as a Professor with the Department of Electrical Engineering, Tokyo University of Science, Tokyo, Japan. His laboratory focuses on sustainable electronics, encompassing low-power artificial intelligence (AI) devices and circuits, sensors and AI signal processing, SOT-RAM and spin-current applications, and quantum computing techniques. Notably, the development of a fully coupled Ising-machine LSI from his group has received significant recognition.

Dr. Kawahara was a recipient of the 9th Yamazaki-Teiichi Prize, in 2009; the IEICE Electronics Society Award, in 2014; and the Prize for Science and Technology (Development Category) in the FY2017 Commendation for Science and Technology by the Japanese Minister of Education, Culture, Sports, Science and Technology. He was the Secretary/Publicity Officer of the 2006/2007 JFE Committee of the Symposium on VLSI Circuits, an IEEE SSCS Distinguished Lecturer, in 2008 and 2009, and the FE Regional Chair of IEEE ISSCC 2009/2010.